Fermi National Accelerator Laboratory

FERMILAB-Conf-75/61-EXP
7100.069

(Submitted to APS Division of Particles
and Fields Meeting in Seattle,
Washington, August 27-29, 1975)

ELASTIC SCATTERING OF $\pi^{\pm}$, $K^{\pm}$, $p^{\pm}$ AT SMALL ANGLES: A PRELIMINARY ANALYSIS

C. Ankenbrandt, M. Atac, R. Brown[†], S. Ecklund, P. J. Gollon,
J. Lach, J. MacLachlan, A. Roberts
Fermi National Accelerator Laboratory
Batavia, Illinois 60510

and

L. A. Fajardo[††], R. Majka, J. N. Marx[†††], P. Nemethy, J. Sandweiss
A. Schiz, A. J. Slaughter
Yale University
New Haven, Connecticut 06520

August 1975

Operated by Universities Research Association Inc. under contract with the Energy Research and Development Administration

ELASTIC SCATTERING OF $\pi^{\pm}$, $K^{\pm}$, $p^{\pm}$ AT SMALL ANGLES: A PRELIMINARY ANALYSIS

C. Ankenbrandt, M. Atac, R. Brown[†], S. Ecklund, P. J. Gollon, J. Lach, J. MacLachlan, A. Roberts
Fermi National Accelerator Laboratory
Batavia, Illinois 60510

and

L. A. Fajardo[††], R. Majka, J. N. Marx[†††], P. Nemethy, J. Sandweiss, A. Schiz, A. J. Slaughter
Yale University
New Haven, Connecticut 06520

ABSTRACT

We present preliminary results from an experiment to measure the small angle elastic scattering of $\pi^{\pm}$, $K^{\pm}$, and $p^{\pm}$ on protons at beam momenta between 50 and 200 GeV/c. The values of ρ, the ratio of the real to imaginary part of the forward scattering amplitude, and b, the exponential slope parameter of the nuclear cross section $d\sigma/dt$, are given for a limited sample of data at 70, 100, 125 and 150 GeV/c.

INTRODUCTION

The study of small angle hadron-proton elastic scattering is a subject of great inherent interest. Dispersion relations, which follow from analyticity, crossing symmetry, and the optical theorem, express the real part of the forward scattering amplitude as an integral of a function of the total cross section over energy. Measurements of the interference between the Coulomb and nuclear scattering amplitude at small angles coupled with the recent accurate total cross section measurements[1] allow a test of dispersion relations up to several hundred GeV.

In Fig. 1 we plot the ratio of the real to imaginary part of the nuclear scattering amplitude, ρ = Re f(0)/Im f(0), at zero four momentum transfer, t, to the target proton. The values of ρ are those computed by Hendrick and Lautrup[2] using dispersion relations and the new total cross section data[1].

The real part of the nuclear scattering amplitude near the forward direction can be determined experimentally from the interference of the strong amplitude with the Coulomb amplitude. Such a measurement requires excellent resolution in the scattering angle, the ability to observe scatters with a $|t| \sim .001$ $(GeV/c)^2$, and a reliable method for the separation of elastic from inelastic events.

In this experiment we measure small angle ($\leq$ 4 mr) elastic scattering of $\pi^{\pm}$, $K^{\pm}$, $p^{\pm}$ on protons at beam momenta between 50 and 200 GeV/c using the M6W beam[3] at Fermilab. The experiment is designed to measure ρ to an accuracy of about 0.01 for $\pi^{\pm}$ and p, and about 0.02 for $K^{\pm}$ and $\bar{p}$. The slope, b, of the

nuclear elastic scattering cross section, $d\sigma/dt$, is determined using an angular range extending to about 4 mr corresponding to a $|t|$ of about 0.12 $(GeV/c)^2$ at 100 GeV/c. In this paper, preliminary results which determine ρ and b from a limited sample of data at 70, 100, 125 and 150 GeV/c beam momenta are presented.

BEAM AND DETECTION APPARATUS

The M6W beam[3] is a three stage beam with each stage having point to parallel to point optics. The second focus is a momentum dispersed focus. A proportional wire chamber (PWC) with 1.0 mm wire spacing placed at this focus determines the momentum of individual beam particles to $\pm$ 0.03%. Momentum and angle are recombined at the third focus located immediately after the magnetic spectrometer. The beam contains three Cerenkov counters; a threshold counter, a DISC, and a differential counter so that all π, K and protons can be identified simultaneously.

The experimental apparatus is depicted in Fig. 2. A pair of high precision PWC's[4] (x and y) separated by 3.5 m measure the particle trajectory incident on a 52 cm long liquid hydrogen target. The scattered particle trajectory is measured by another pair of high precision PWC's separated by 4.5 m. The group immediately following the target contains two additional chambers (u and v) rotated by 45° for redundancy. Each of these high precision PWC's is composed of two staggered planes giving an effective wire spacing of 0.2 mm and a measured resolution of 70 μm (σ). All high precision chambers are mounted on a steel reinforced concrete block to ensure stability. The scattering angle is determined to 40 μr by these chambers.

Lead and scintillation counters surround the target and are used in the off-line analysis to help discriminate against inelastic events.

The concrete block is followed by two main-ring bending magnets which serve to momentum analyze the scattered particles. Conventional PWC's are located immediately following (1.5 mm wire spacing) and 30 meters downstream of the magnets (a pair of staggered planes with 1.0 mm effective wire spacing). The resolution of the system due to both chamber resolution and multiple scattering is given in Fig. 3. An elastic constraint to better than one pion mass is achieved for beam momenta up to 150 GeV/c.

The regions between the high precision PWC's as well as the spectrometer magnet apertures are evacuated to minimize scattering. A low pressure (5 PSIA at 100 GeV/c) helium filled threshold Cerenkov counter is located between the two clusters of PWC's after the spectrometer magnets.

The final downstream elements of the system are a lead-scintillator shower detector for electron identification and an iron-scintillator calorimeter for muon identification. Typically the lepton component of the beam, which varies with momentum, is several percent. Muon identification is also important to help identify π and K decays which can simulate scatters in the target region.

TRIGGER AND RATES

Data acquisition is triggered by a two level system consisting of a scintillation counter pretrigger and a fast analog processor which identifies scattered events from the

wires struck in the PWC's before and after the hydrogen target.

The scintillation counter pretrigger consists of two small beam defining counters (B1 and B2) and a hole veto (VH1) at the upstream end of the concrete block, a 15- x 30-cm counter (S) in front of the most downstream PWC in the experiment and a small beam veto (V) located at the beam focus at the downstream end of the spectrometer magnets. The beam veto, whose size depends on the beam momentum, was chosen such that no scatters with $|t| > 0.001$ $(GeV/c)^2$ are rejected. The pretrigger for scattered events is

$$B1 \cdot B2 \cdot \overline{VH1} \cdot \overline{V} \cdot S$$

while the pretrigger for incident beam particles is

$$B1 \cdot B2 \cdot \overline{VH1}$$

Depending on the beam momentum between 50% and 90% of the incident beam is rejected by the scattered event pretrigger. The output of B1 is also used to ration the beam so the RF buckets with more than one particle, or neighboring buckets which are occupied are rejected.

Scattered particle pretriggers initiate the fast analog processor which scans the high precision PWC readout. The processor is described elsewhere[5]. Data from the two high precision PWC's upstream of the hydrogen target are used to perform two calculations in parallel.

Firstly, the incident trajectory is projected to the plane of the beam veto. If the projection lies outside of the veto counter the pretrigger is rejected. This process selects those particles in the incident beam phase space which would strike

the beam veto if they are not deflected by material in the region of the hydrogen target.

Secondly, the incident trajectory is projected to the plane of the high precision PWC just upstream of the magnetic spectrometer. If the projected hit and the actual hit differ by less than a specified amount the pretrigger is rejected. This specified amount is a function of the incident momentum and selected to correspond to $|t| \sim 0.001$ $(GeV/c)^2$.

This on-line analog processor thus rejects particles outside of the desired incident beam phase space (halo) and unscattered beam particles. In Fig. 4 we present the $\sqrt{-t}$ distribution of a small sample of scattered triggers at 70 GeV/c. The figure illustrates the efficiency of the scattered trigger in eliminating the unscattered beam without rejecting scatters in the region of interest.

* In addition to scattered triggers, we trigger on a prescaled number of incident beam particles. Accurate normalization can thus be achieved by requiring both scattered and unscattered particles to pass through the same detectors.

Data taking is typically carried out with a raw beam intensity of $6 \cdot 10^5$ particles per accelerator pulse. The data collection system is capable of recording about 800 events per pulse. However, the running time at each momentum is determined by the available intensity of the rarer particles, (K^-, $\bar{p}$ or K^+) depending on the beam polarity. To enhance the yield of the rarer particles, we scaled down the trigger rate of the predominant particles, (π^- or π^+, p). This resulted in about a 60% live time and an effective rationed beam of

$4 \cdot 10^4$ particles per pulse. Of these the scattered trigger accepted ~ 0.4%. These rates result in about 20 elastic scatters per pulse inside of the acceptance of the apparatus, of which 10 events pass the off-line cuts described in the next section. The goal of the data taking is 10^5 events for $\pi^{\pm}$ and p and $5 \cdot 10^4$ events for $K^{\pm}$ and $\bar{p}$ at each beam energy.

ANALYSIS

The separation of elastic scatters from scattered triggers requires the following series of off-line cuts:

1. Wire cluster cut. All events are required to have one and only one cluster of struck wires in the X and Y high precision PWC's, the upstream momentum tagging chamber and the 1.0 mm effective wire spacing PWC at the end of the magnetic spectrometer. The single clusters have no more than three contiguous wires hit. This cut eliminates approximately 50% of the triggers. We note that a similar cut imposed on unscattered events preserves the accurate normalization.
2. Lepton cut. Events are also required to give a low pulse height in the electron shower counter and a large pulse height in the iron-scintillator calorimeter.
3. Fiducial volume cut. Scattered tracks are required to have an interaction vertex in the liquid hydrogen target volume. The reconstructed vertex position along the beam line at 70 GeV/c incident momentum is depicted in Fig. 5 and Fig. 6 for target full and target empty runs. Scattering in the PWC's is clearly separable from target scattering. A second cut, imposed at

the veto plane (V) to define the apertures of the system, eliminates a negligible number of events.

4. Electron scattering cut. Beam particles scattered from electrons in the liquid hydrogen target are separated from proton scatters by kinematic constraints and a latched hole veto just downstream of the target (not shown in Fig. 2). If a recoil mass (RM) is constructed assuming a proton target, electron target events have an $RM^2 > 2.0\ GeV^2$ for $-t > 0.002\ (GeV/c)^2$. We apply an $RM^2 < 1.7\ GeV^2$ cut to eliminate the target electron scatters from the elastic sample. The hole veto in conjúnction with a cut on the recoil mass calculated assuming an electron target separates the beam target electron scatters from the inelastic sample.

5. Inelastic scatter cut. Inelastic scatters are eliminated from the elastic sample by requiring the $RM^2 < 1.7\ GeV^2$ and that there be no hits in any of the lead scintillation veto counters surrounding the target. The counters, which are latched with each trigger, are sensitive to gammas from π^o's produced if the target proton is excited in an inelastic collision as well as directly produced charged particles. Figure 7 depicts the RM^2 distribution for pp events at 70 GeV/c after beam target electron scatters have been removed. The width of the elastic peak reflects the resolution ($\Delta p/p \sim 0.09\%$) of the system in measuring the momentum change of the projectile in the interaction.

After the above cuts have isolated the elastic scatters, a target empty subtraction is applied. A qualitative appreciation for the subtraction correction can be gained by using the chamber scattering to obtain the relative normalization of target empty to target full. See Fig. 5 and 6. In the analysis incident beam is used to give the relative normalization. The two methods agree, giving a target empty subtraction of < 4%.

We analyze our data in terms of the variable $\sqrt{-t}$ which at these energies closely approximates $P_\perp$ for elastic events. Among the virtues of this variable is that our resolution is only weakly dependent upon it, and our data is almost flat when binned in constant intervals of $\sqrt{-t}$. This means that the transfer of events into adjacent bins due to our resolution will not be as severe a correction compared to using a variable which has a steeper cross section dependence.

Before fitting the data we must correct for the geometric acceptance of the detection apparatus. An approximate analytic calculation of the acceptance was used to obtain the preliminary results presented here. In this simplified computation the lower limit of $\sqrt{-t}$ was 0.05 GeV/c and the upper limit corresponded to a scattering angle of about 2.5 mr, equivalent to $\sqrt{-t}$ = 0.17 at 70 GeV/c. The analytic acceptance calculation does not fully account for all of the apertures in the apparatus, thus increasing our systematic errors. However, the limited range of $\sqrt{-t}$ does significantly hinder an accurate determination of b. The final analysis of the complete data sample will include a Monte-Carlo simulation

of the full acceptance of the apparatus in $\sqrt{-t}$. This simulation will include the effects of Coulomb scattering (plural and multiple), and detector resolution. It will use a beam phase space distribution taken from measured incident beam tracks. This preliminary analysis does, however, include a first order correction for multiple scattering and detector resolution.

The measured angular distribution of elastic events for each projectile ($\pi^{\pm}$, $K^{\pm}$ or $p^{\pm}$) at each beam momentum is fit to the expected form of the differential cross section,

$$\frac{d\sigma^{\pm}}{d(-t)^{\frac{1}{2}}} = \frac{8\pi\alpha^2 G^2(t)}{(-t)^{3/2}} + \frac{(1+\rho_{\pm}^2)\,\sigma_T^2\, e^{bt}\,(-t)^{\frac{1}{2}}}{8\pi}$$

$$\mp \frac{2\,G(t)\,\sigma_T\, e^{bt/2}}{(-t)^{\frac{1}{2}}}\left[2\rho_{\pm}\cos 2\delta \pm \sin 2\delta\right]$$

where t is the invariant four momentum transfer, α is the fine structure constant, G(t) the product of the electromagnetic form factors of the hadrons, δ the Coulomb phase angle[6], and ρ the ratio of real to imaginary parts of the nuclear scattering amplitude. For this preliminary analysis we have set all hadronic form factors to one. The subscript + or - denotes the electric charge of the projectile.

The values for ρ presented in this paper are obtained by fitting to the form given above. Incorporated in the fit with their errors are the recent Fermilab total cross section measurements[1]. Since the unstattered beam passes through the same detectors as the scattered beam, corrections for effects such as detector inefficiencies and absorption are common to both and so, to first order, cancel in the normalization. In

the preliminary fits we have used a conservative estimate of 5% for the uncertainty in the normalization.

PRELIMINARY RESULTS

Figure 8 depicts the differential cross section, $d\sigma/dt$ for $\pi^- p$ elastic scattering at 70 GeV/c and the best fit to the data. This plot contains only 10% of the full data sample for only one beam particle at one energy. At each energy we have measured $d\sigma/dt$ for 6 particles ($\pi^\pm$, $K^\pm$, $p^\pm$ on protons). The full data sample is expected to be 50,000 events for $K^\pm$ and $\bar{p}$ and $\geq$ 100,000 events for $\pi^\pm$ and p at each energy.

The results of the preliminary analysis of a small fraction of the full data sample are given in Table I. Results for the ratio of real to imaginary part of the nuclear amplitude (ρ) and the nuclear slope parameter (b) for several energies are presented. The error on b will decrease when a better understanding of the geometric acceptance allows us to fit to larger values of $\sqrt{-t}$. The table also includes the number of events used in the analysis and the Chi-squared per degree of freedom of the best fit. All quoted uncertainties are statistical.

In Fig. 9 we present dispersion relation predictions with data from other experiments, and the results from Table I. The 70 GeV/c data has the smallest t acceptance and here in particular the results are very sensitive to our acceptance calculation. With this in mind we believe our data to agree with the theoretical predictions, within our statistical and systematic uncertainties. We wish to point

out the scarcity of data for $K^{\pm}$, $\bar{p}$ and $\pi^{\pm}$ above Serpukhov energies.

The slope parameter, b, will be determined in the full range of $\sqrt{-t}$ shown in Fig. 10. We note that the discontinuity observed in pp elastic scattering at high energies occurs at $\sqrt{-t} \sim 350$ MeV/c. This value of $\sqrt{-t}$ falls within our acceptance for beam momenta of 100 GeV/c and higher. It will be interesting to see if such a break also occurs in meson-proton elastic scattering.

Care has been taken not to bias our data sample against inelastic events. The only scintillation counter downstream of the hydrogen target used in anti-coincidence is our small veto counter (V). All of the other scintillation counters are latched so that in the off-line analysis the inelastic events can be separated from the elastic events. We should be able to study the fragmentation of the target proton at small $|t|$ as a function of incident energy and particle type.

ACKNOWLEDGMENTS

We wish to thank our engineering staff, Michael Catalano, Satish Dhawan, Andy Disco, Cordon Kerns, Peter Martin, and Irving Winters and our technicians, Jon Blomquist, Kevin Dolan, Garvey Hale and Ed Steigmeyer for their help in the design, setup and maintenance of the apparatus. Without the dedicated help of the Meson Department staff this experiment would not have been possible.

† Visitor from Rutherford Laboratory, Chilton, Didcot, Berkshire, England

†† Ford Foundation Doctoral Fellow

††† Jr. Faculty Fellow

REFERENCES

[1] A. S. Carroll et al., Fermilab-Pub-75/51-EXP 7100.104.

[2] R. E. Hendrick and B. Lautrup, Phys. Rev. D11, 529 (1975)

[3] J. R. Orr and A. L. Read, Meson Laboratory Preliminary Design Report, March 1971, Fermilab.

[4] S. Dhawan et al., submitted to Nuclear Inst. & Methods.

[5] S. Dhawan and R. Majka, IEEE Transactions on Nuclear Science, NS-22, 303 (1975).

[6] B. West and D. R. Yennie, Phys. Rev. 172, 1413 (1968). We use their parameterization of the Coulomb phase angle with b = 8 $(GeV/c)^2$.

$$\delta = \alpha \ln \left(\frac{0.268 \text{ GeV/c}}{\sqrt{-t}} \right)$$

TABLE I

Particle	Incident Momentum (GeV/c)	ρ	$b(GeV/c)^{-2}$	Number of Events (K)	χ^2 Per Degrees of Freedom
π^-	70	-0.14 ± 0.05	7.3 ± 2.2	9.8	28./21
	100	0.00 ± 0.08	11.5 ± 1.6	7.2	69./35
	125	0.05 ± 0.05	9.7 ± 0.6	13.5	28./22
	150	-0.03 ± 0.05	9.6 ± 0.5	13.9	39./27
π^+	70	0.09 ± 0.05	10.4 ± 2.0	8.2	22./21
	100	0.02 ± 0.09	10.1 ± 1.8	6.7	78./35
	125	-0.01 ± 0.05	9.3 ± 0.7	12.2	56./47
	150	-0.08 ± 0.05	9.2 ± 0.4	13.5	70./60
K^-	70	-0.16 ± 0.07	7.2 ± 3.5	2.1	35./21
	100	-0.06 ± 0.10	9.2 ± 2.0	3.9	73./35
	125	0.03 ± 0.05	9.8 ± 0.6	7.7	20./22
	150	0.10 ± 0.08	9.2 ± 0.6	7.3	48./27
K^+	70	0.04 ± 0.07	8.5 ± 3.7	0.9	23./21
	100	0.13 ± 0.10	11.6 ± 2.2	2.8	66./35
	125	0.08 ± 0.07	9.3 ± 1.1	3.7	66./47
	150	-0.02 ± 0.06	8.3 ± 0.5	3.8	40./60
$\bar{p}$	70	-0.11 ± 0.06	8.2 ± 2.1	5.4	20./21
	100	0.02 ± 0.10	13.5 ± 1.6	6.2	61./35
	125	0.08 ± 0.08	12.2 ± 0.6	8.0	31./22
	150	-0.08 ± 0.10	12.5 ± 0.6	5.0	34./27
p	70	-0.07 ± 0.06	9.5 ± 2.0	8.9	32./21
	100	-0.20 ± 0.14	9.2 ± 1.7	10.8	142./35
	125	-0.07 ± 0.06	12.0 ± 0.5	20.0	61./47
	150	-0.10 ± 0.06	11.2 ± 0.3	24.8	72./60

FIGURE CAPTIONS

1. ρ = ratio of the real to the imaginary part of the nuclear scattering amplitude at t = 0, from reference 2.
2. Experimental apparatus.
3. (a) Resolution in $\sqrt{-t}$. Note that $\sqrt{-t} = p_\perp$.
   (b) Resolution in momentum measurement of the outgoing track.
4. $\sqrt{-t}$ distribution for a sample of scattered triggers which pass the wire cluster cut.
5. Target full Z distribution for all scattered triggers after wire cluster cut.
6. Target empty Z distribution for all scattered triggers after the the wire cluster cut.
7. Recoil mass squared spectrum for pp at 70 GeV/c. The wire cluster cut, Z cut, and beam target electron scattering cuts have been applied.
8. $d\sigma/dt$ for $\pi^- p$ elastic scattering at 70 GeV/c. The solid line is the best fit to the data.
9. Figure 1 repeated with preliminary results indicated.
10. Momenta and $\sqrt{-t}$ range covered in this experiment. Solid lines are data in hand; dashed lines, 175, 200 and 50 GeV/c, are future runs.

Figure 1

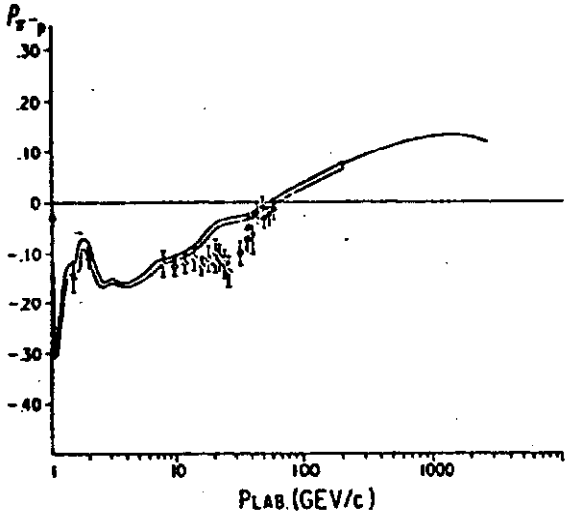
$\rho_{\pi^- p}$
.30
.20
.10
0
-.10
-.20
-.30
-.40
1
10
100
1000
PLAB. (GEV/c)

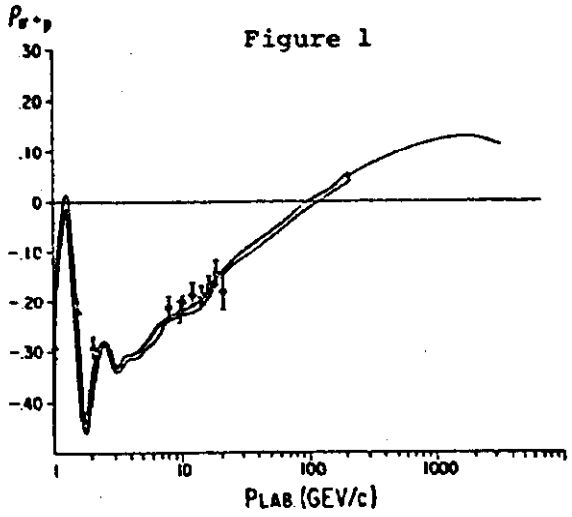
$\rho_{\pi^+ p}$
.30
.20
.10
0
-.10
-.20
-.30
-.40
1
10
100
1000
PLAB. (GEV/c)

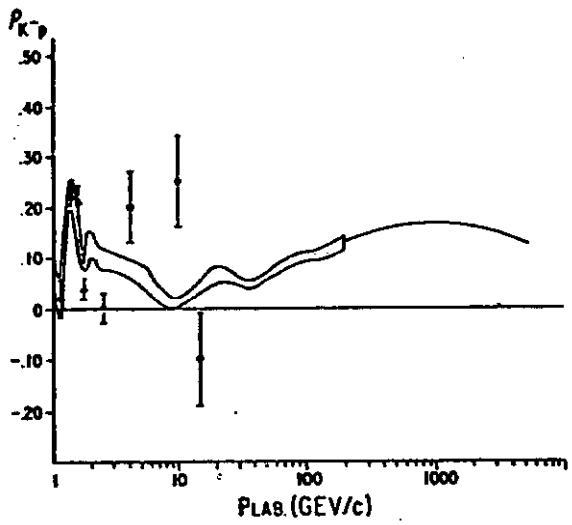
$\rho_{K^- p}$
.50
.40
.30
.20
.10
0
-.10
-.20
1
10
100
1000
PLAB. (GEV/c)

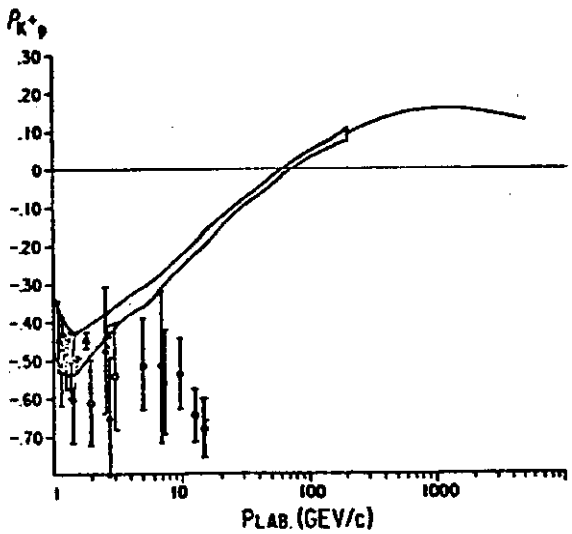
$\rho_{K^+ p}$
.30
.20
.10
0
-.10
-.20
-.30
-.40
-.50
-.60
-.70
1
10
100
1000
PLAB. (GEV/c)

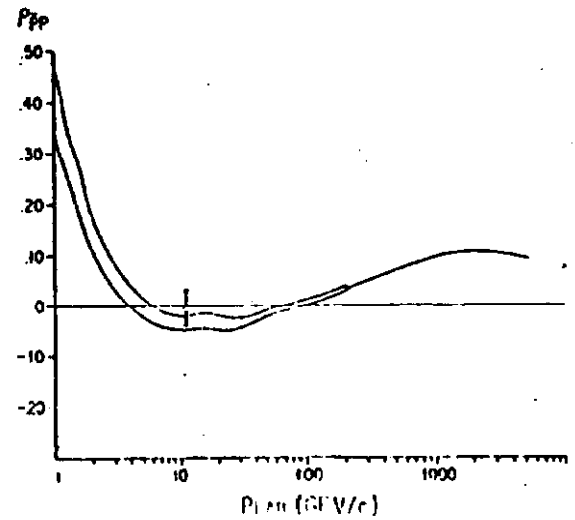
ρ_{pp}
.50
.40
.30
.20
.10
0
-.10
-.20
1
10
100
1000

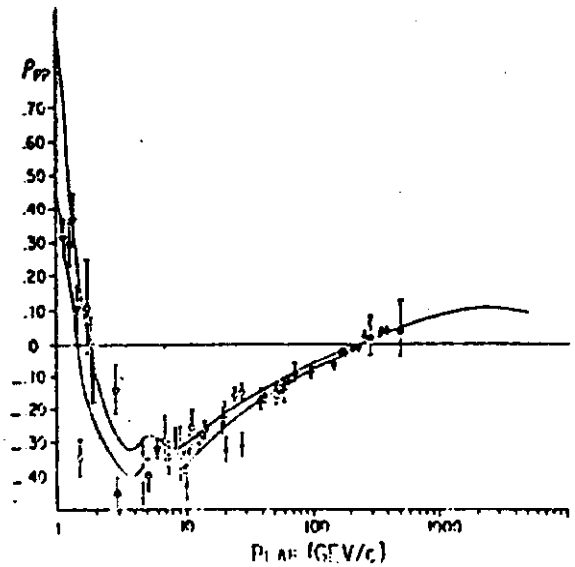
ρ_{pp}
.70
.60
.50
.40
.30
.20
.10
0
-.10
-.20
-.30
-.40
1
10
100

Figure 2

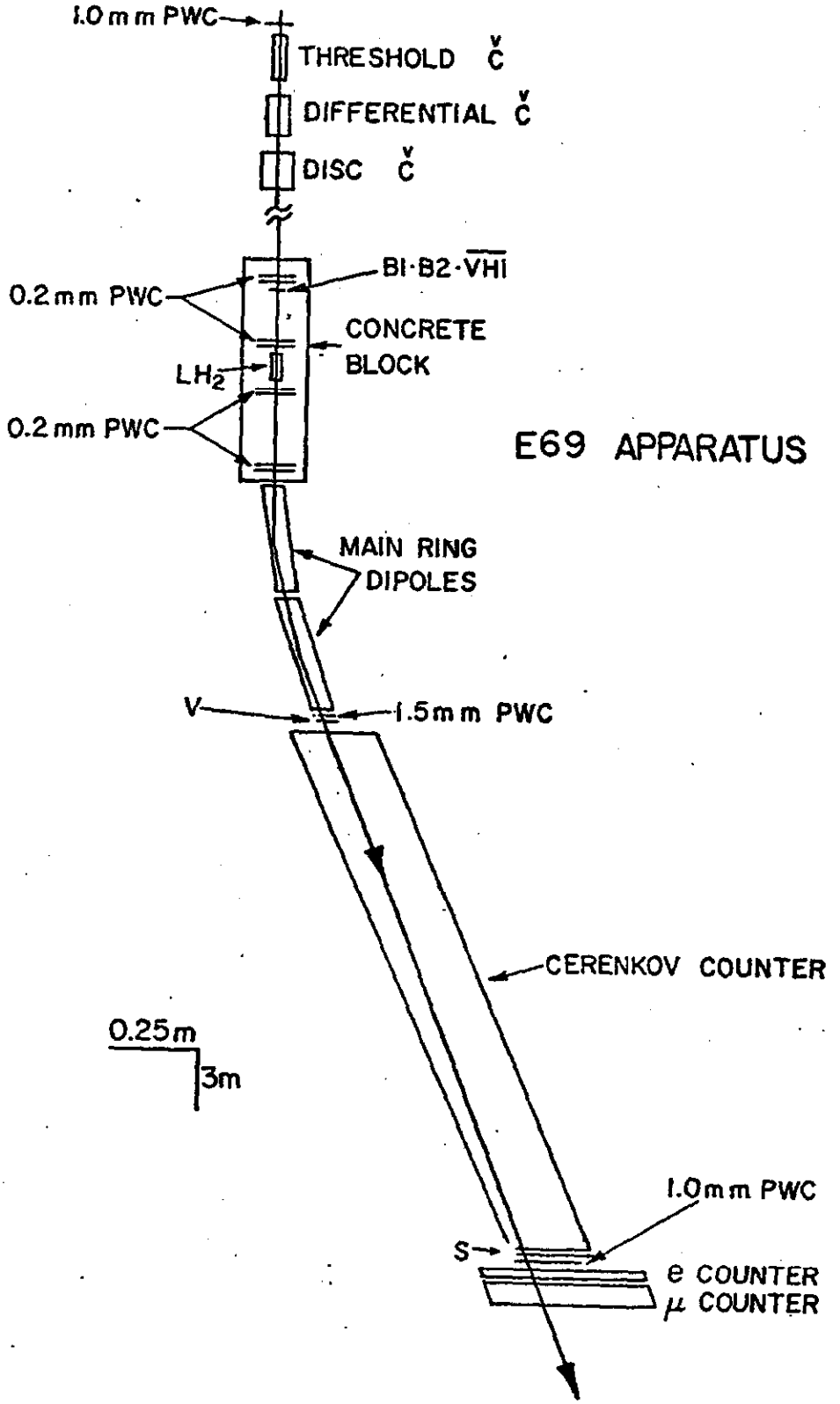
1.0 mm PWC
THRESHOLD $\check{C}$
DIFFERENTIAL $\check{C}$
DISC $\check{C}$
B1·B2·$\overline{VH1}$
0.2 mm PWC
CONCRETE BLOCK
LH_2
0.2 mm PWC
E69 APPARATUS
MAIN RING DIPOLES
V
1.5 mm PWC
CERENKOV COUNTER
0.25m
3m
1.0 mm PWC
S
e COUNTER
μ COUNTER

Figure 3

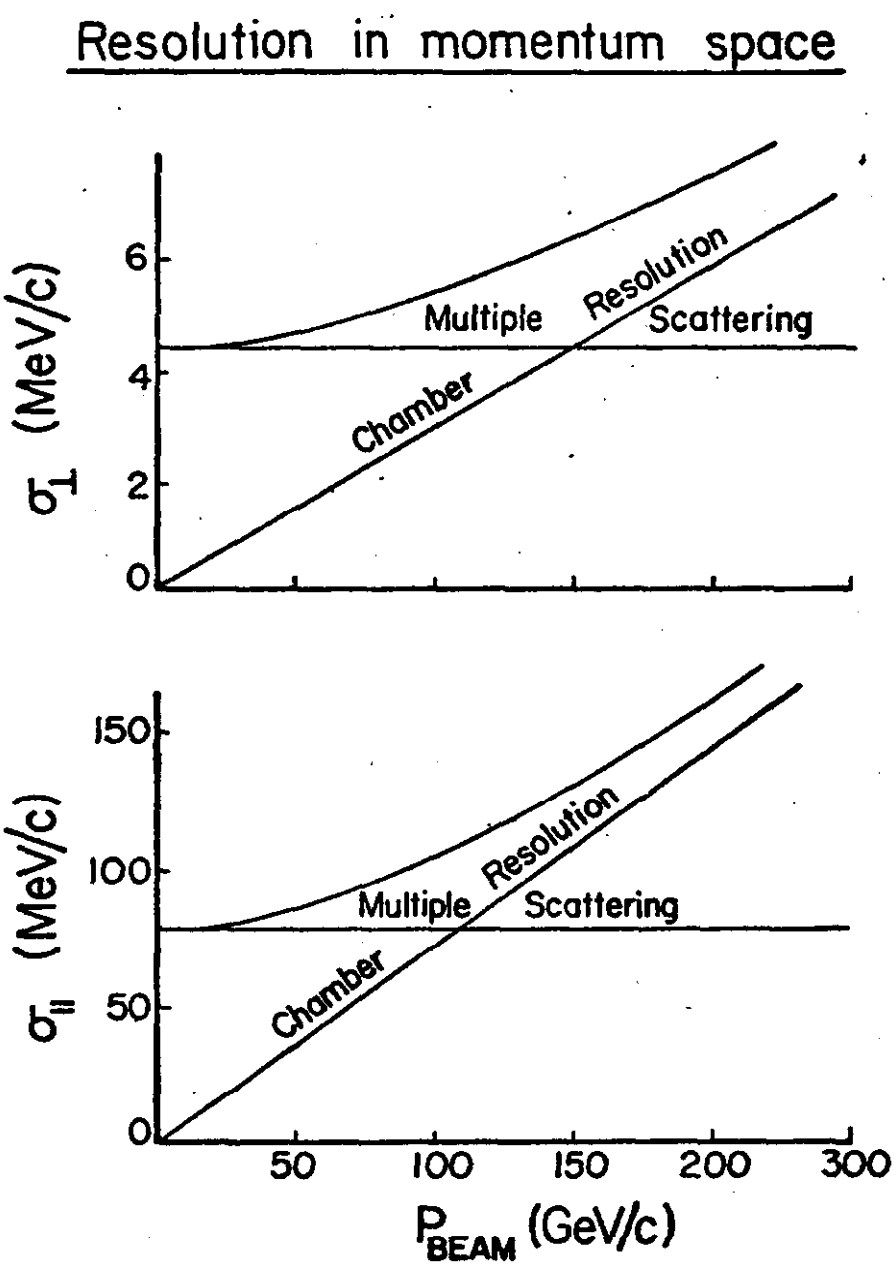
Resolution in momentum space
6
4
2
0
$\sigma_\perp$ (MeV/c)
Multiple Scattering
Resolution
Chamber
150
100
50
0
$\sigma_{\parallel}$ (MeV/c)
Multiple Scattering
Resolution
Chamber
50
100
150
200
300
P_{BEAM} (GeV/c)

Figure 4

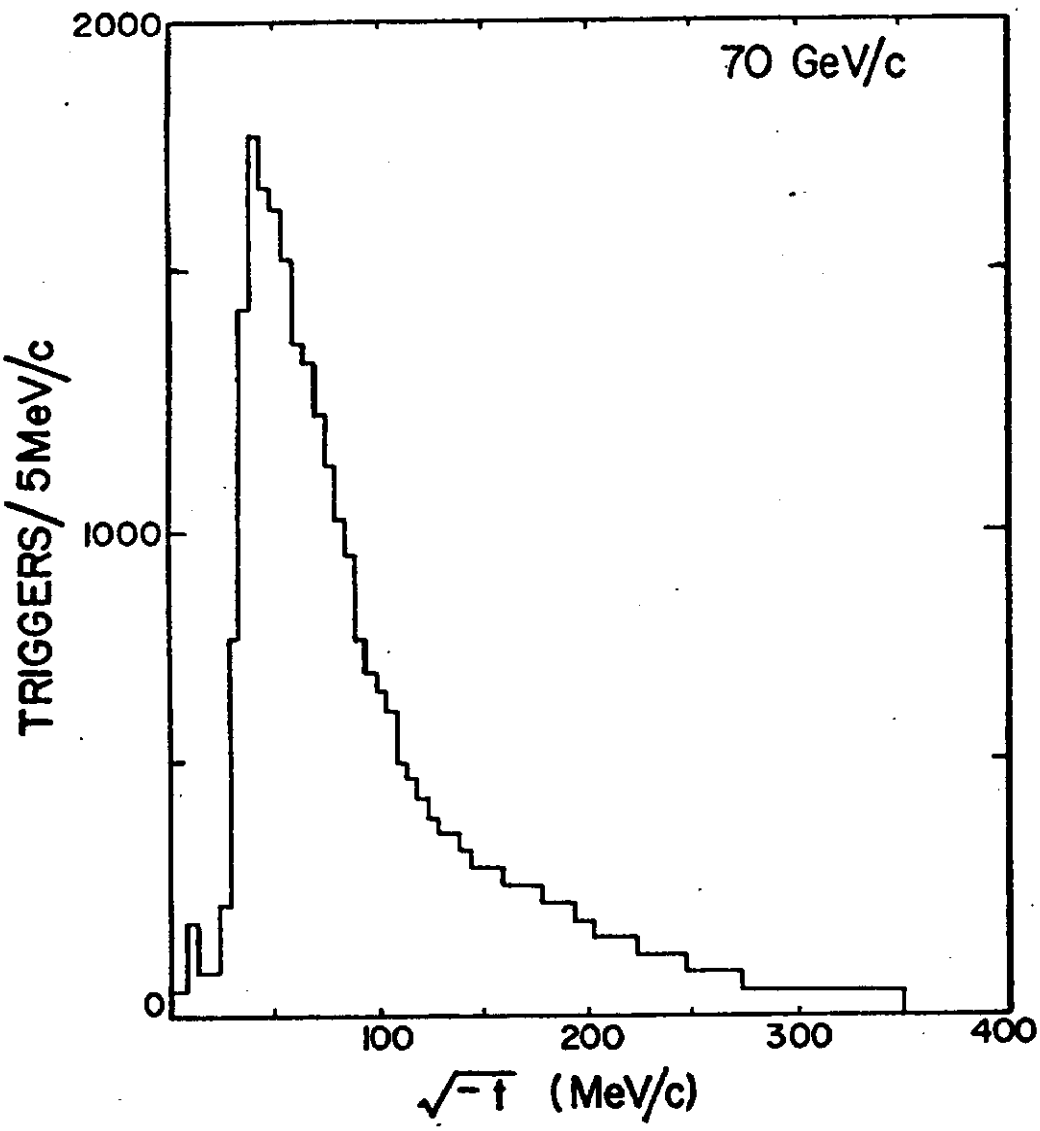

Figure 5

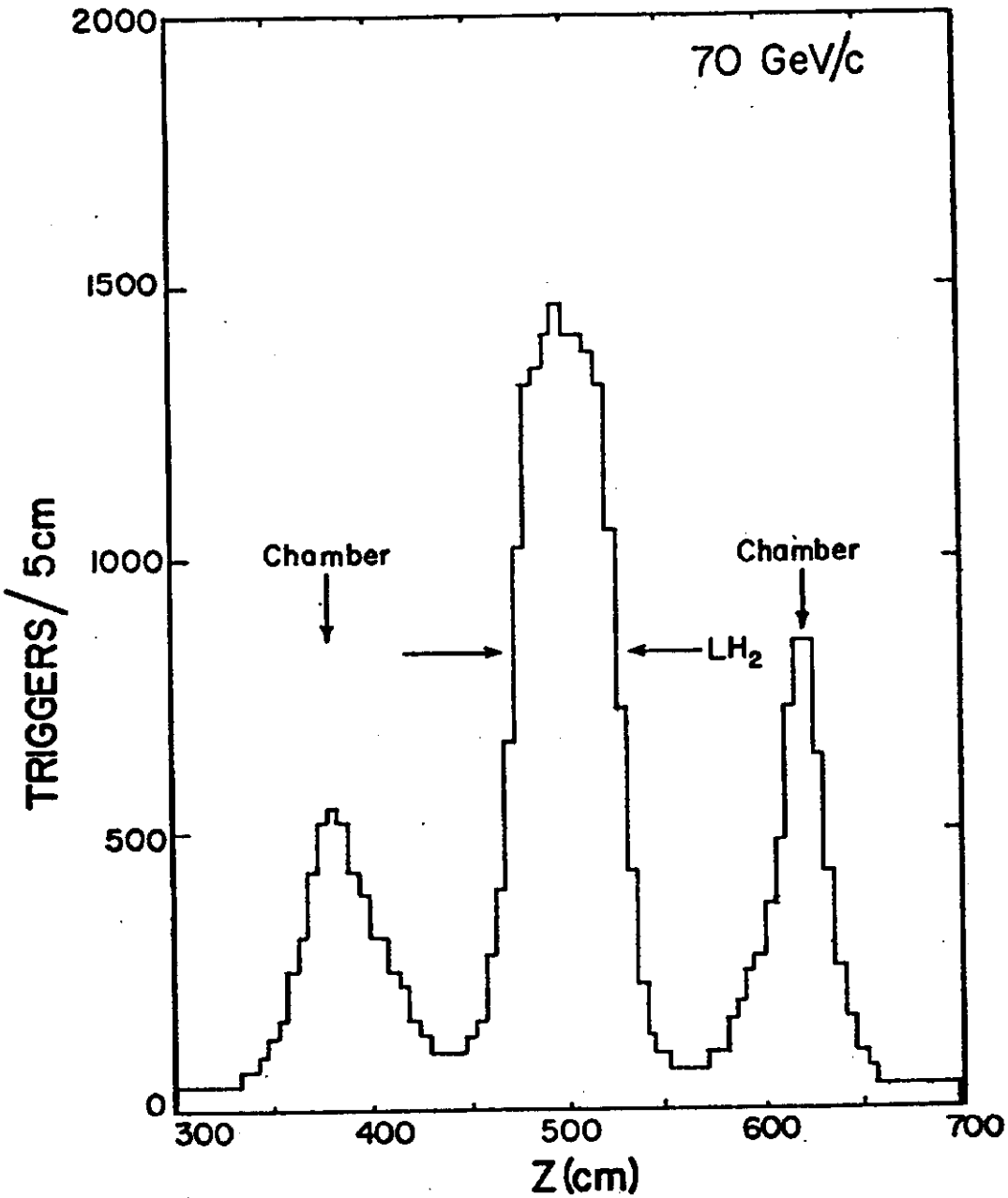
70 GeV/c
2000
1500
1000
500
0
TRIGGERS / 5cm
Chamber
Chamber
LH2
300
400
500
600
700
Z (cm)

Figure 6

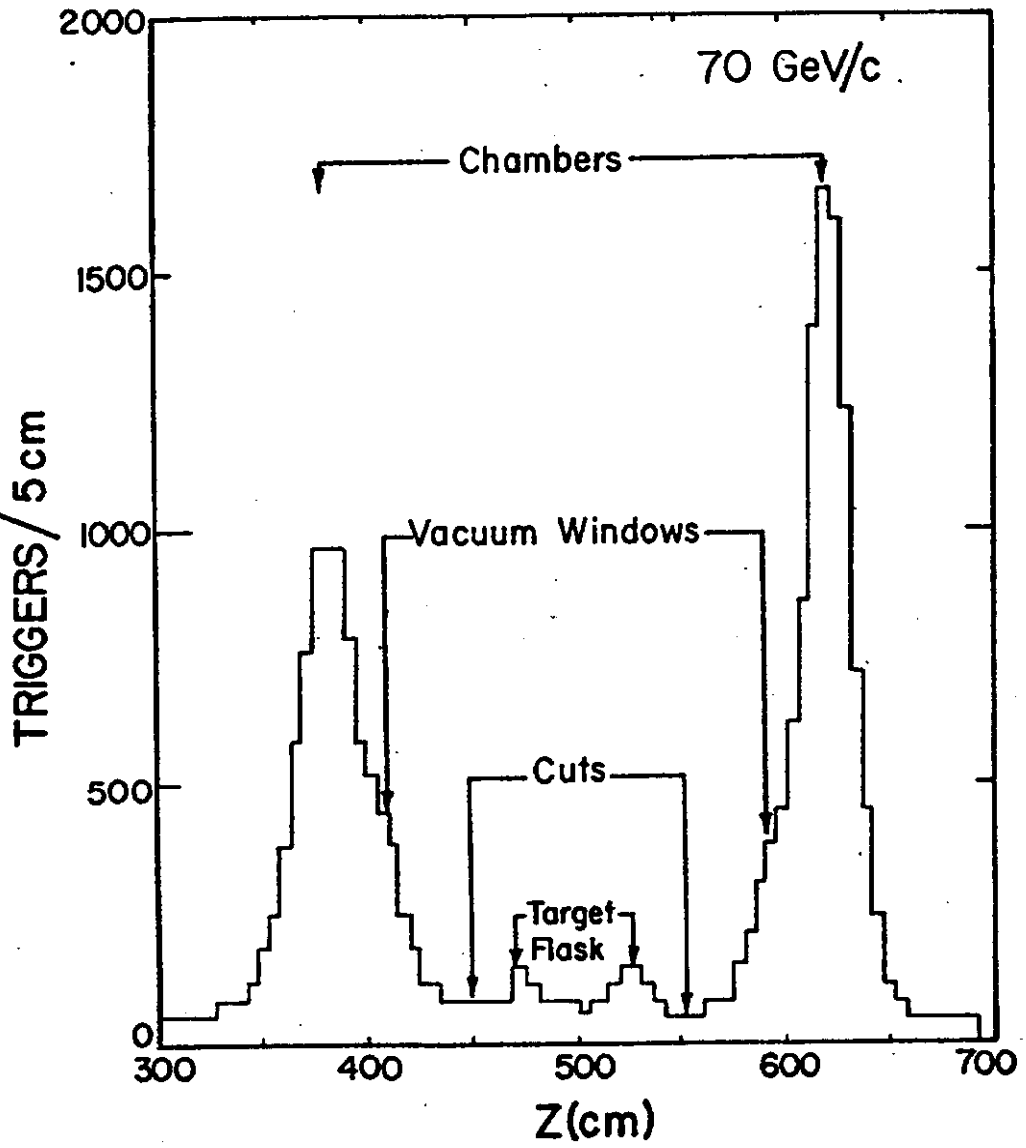
70 GeV/c
Chambers
Vacuum Windows
Cuts
Target
Flask
TRIGGERS/5cm
Z(cm)
2000
1500
1000
500
0
300
400
500
600
700

FIGURE 7

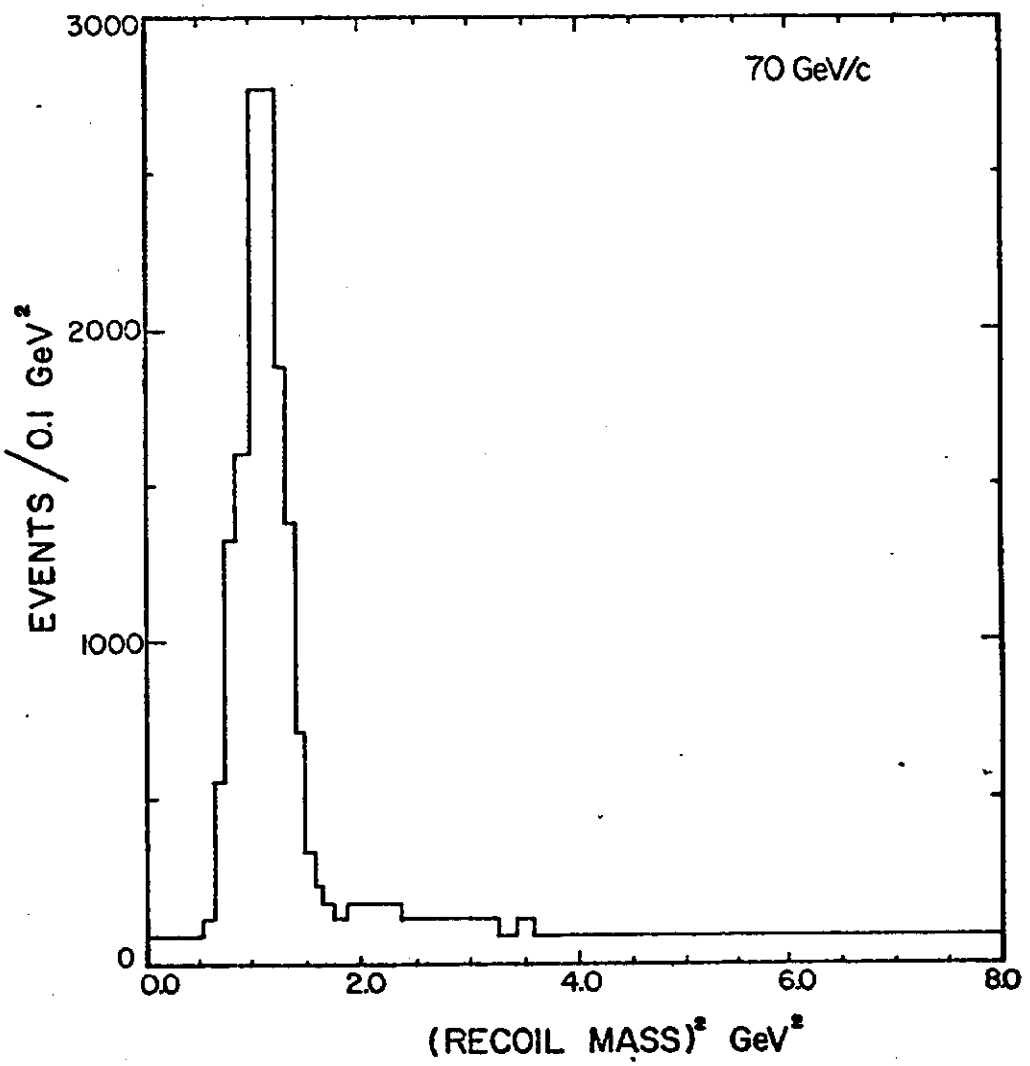
70 GeV/c
EVENTS /0.1 GeV²
3000
2000
1000
0
0.0
2.0
4.0
6.0
8.0
(RECOIL MASS)² GeV²

FIGURE 8

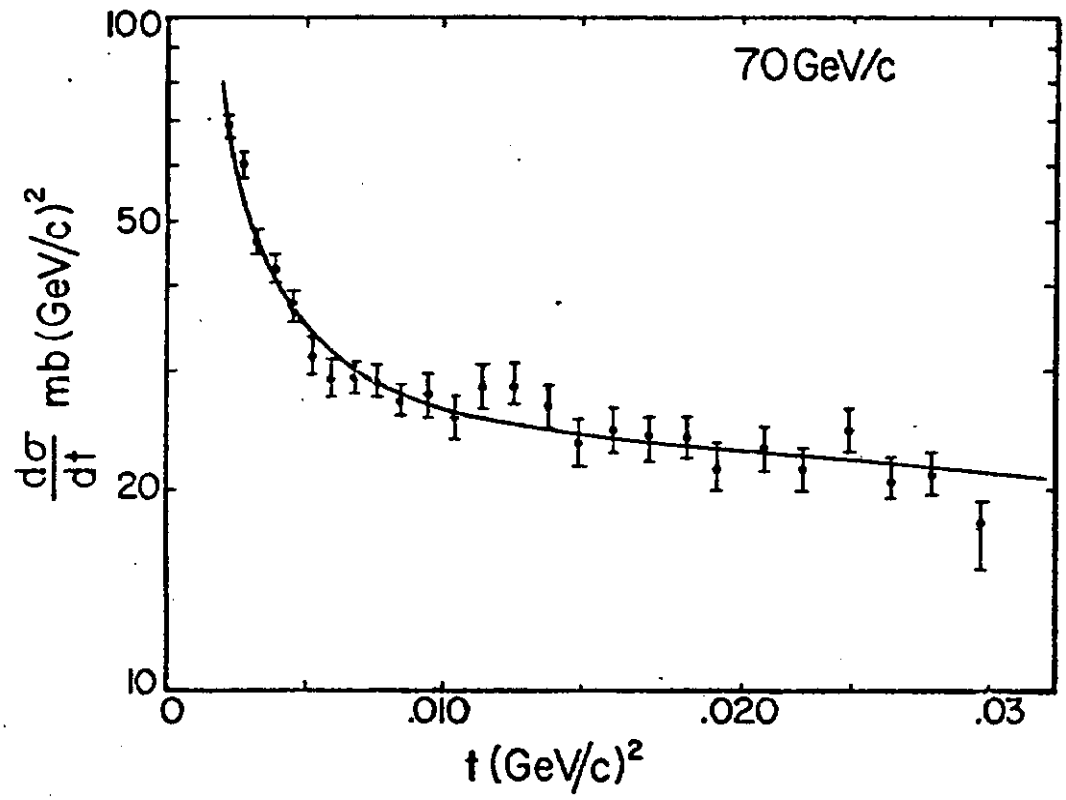

Figure 9

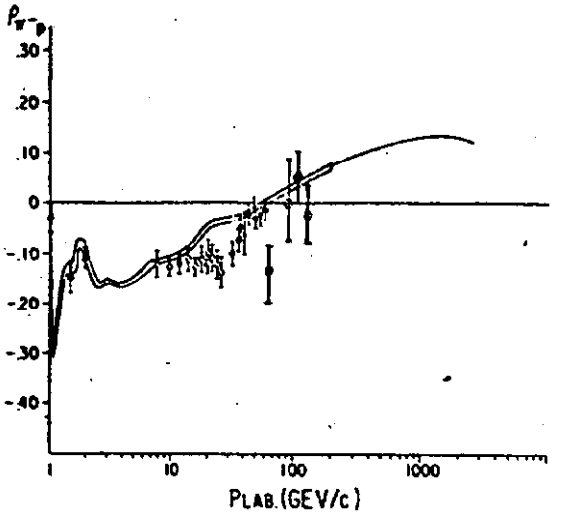
$P_{\pi^- p}$
.30
.20
.10
0
-.10
-.20
-.30
-.40
1
10
100
1000
PLAB.(GEV/c)

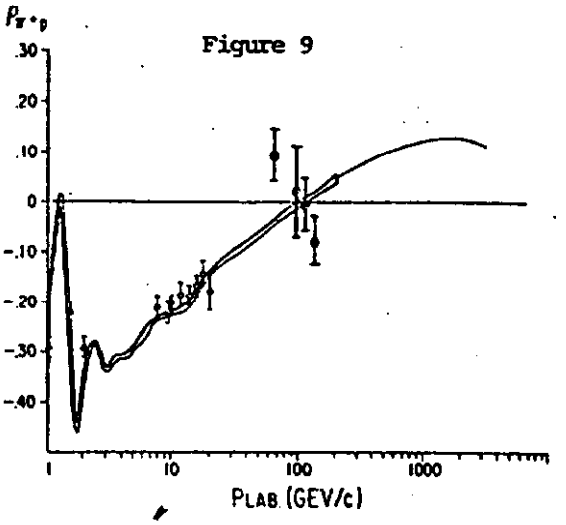
$P_{\pi^+ p}$
.30
.20
.10
0
-.10
-.20
-.30
-.40
1
10
100
1000
PLAB.(GEV/c)

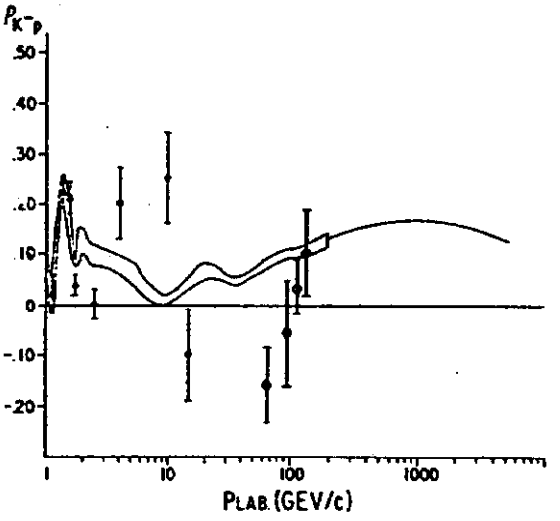
$P_{K^- p}$
.50
.40
.30
.20
.10
0
-.10
-.20
1
10
100
1000
PLAB.(GEV/c)

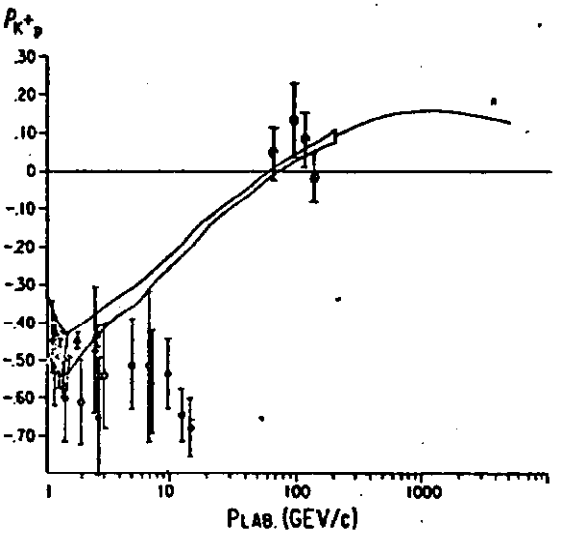
$P_{K^+ p}$
.30
.20
.10
0
-.10
-.20
-.30
-.40
-.50
-.60
-.70
1
10
100
1000
PLAB.(GEV/c)

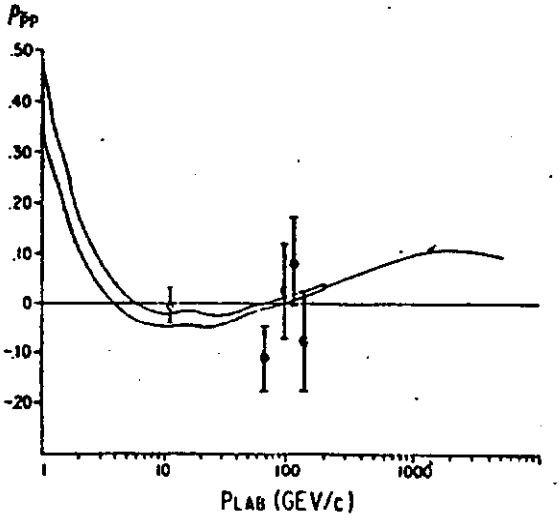
P_{pp}
.50
.40
.30
.20
.10
0
-.10
-.20
1
10
100
1000
PLAB (GEV/c)

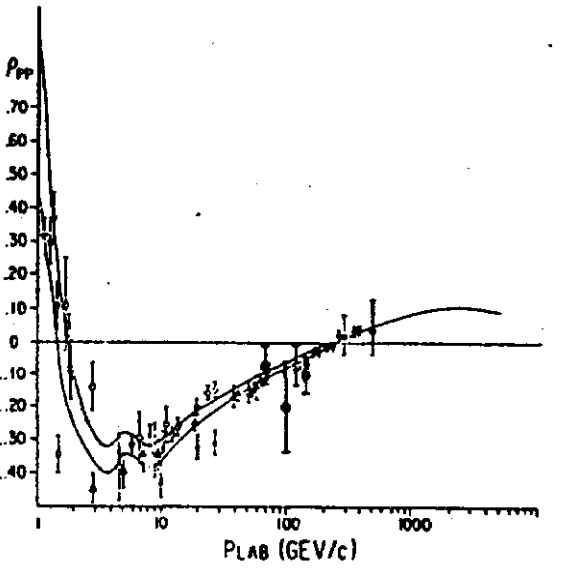
P_{pp}
.70
.60
.50
.40
.30
.20
.10
0
-.10
-.20
-.30
-.40
1
10
100
1000
PLAB (GEV/c)

Figure 10

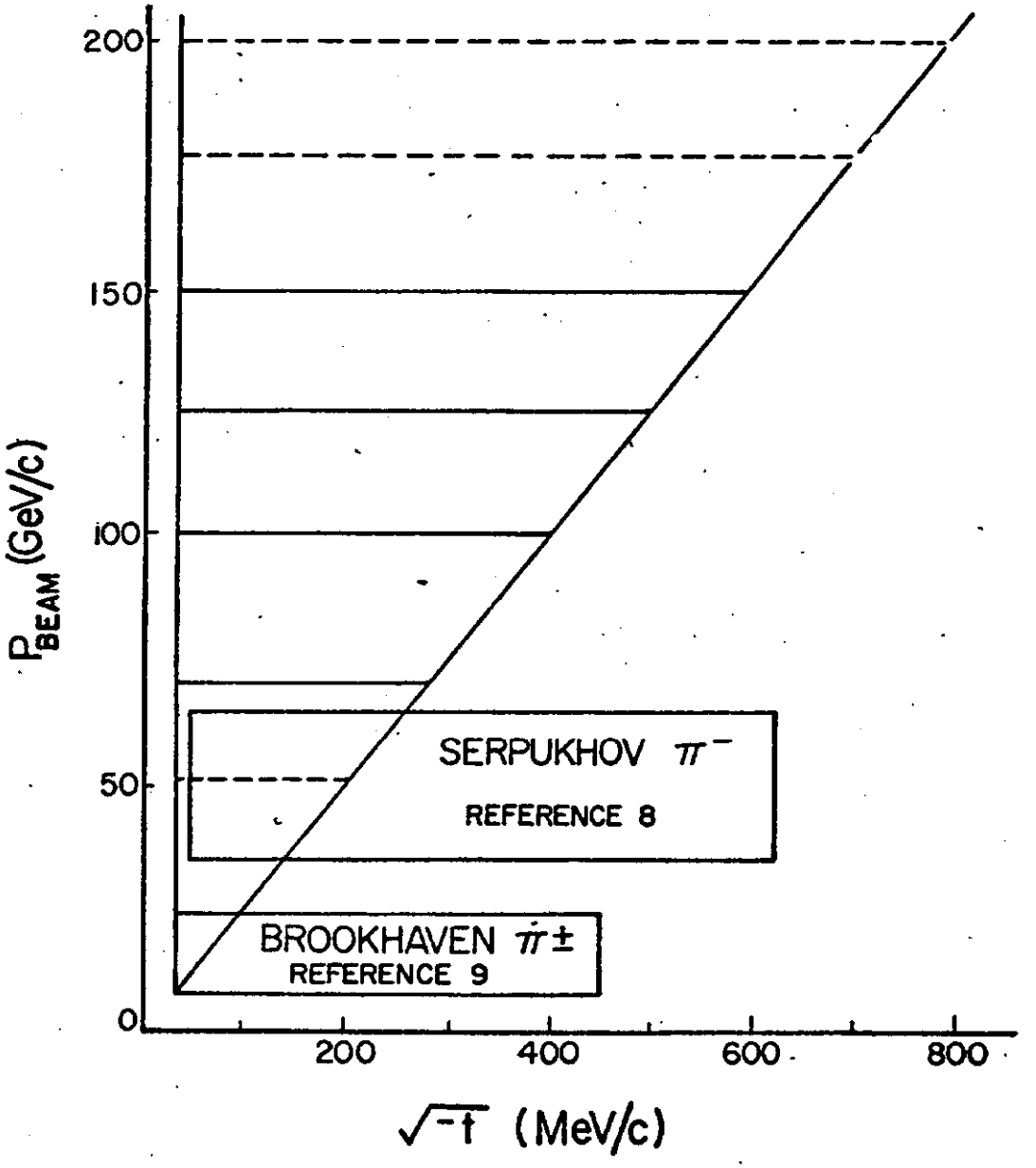
200
150
100
50
0
P_{BEAM} (GeV/c)
SERPUKHOV π^-
REFERENCE 8
BROOKHAVEN $\pi^\pm$
REFERENCE 9
200
400
600
800
$\sqrt{-t}$ (MeV/c)